Extended Transiting Disks and Rings Around Planets and Brown Dwarfs: Theoretical Constraints

J. J. Zanazzi[1]*, and Dong Lai[1]

[1]*Cornell Center for Astrophysics, Planetary Science, Department of Astronomy, Cornell University, Ithaca, NY 14853, USA*

12 October 2016

ABSTRACT
Newly formed planets (or brown dwarfs) may possess disks or rings that occupy an appreciable fraction of the planet's Hill sphere and extend beyond the Laplace radius, where the tidal torque from the host star dominates over the torque from the oblate planet. Such a disk/ring can exhibit unique, detectable transit signatures, provided that the disk/ring is significantly misaligned with the orbital plane of the planet. There exists tentative evidence for an extended ring system around the young K5 star 1 SWASP J140747-354542. We present a general theoretical study of the inclination (warp) profile of circumplanetary disks under the combined influences of the tidal torque from the central star, the torque from the oblate planet and the self-gravity of the disk. We calculate the equilibrium warp profile ("generalized Laplace surface") and investigate the condition for coherent precession of the disk. We find that to maintain non-negligible misalignment between the extended outer disk and the planet's orbital plane, and to ensure coherent disk precession, the disk surface density must be sufficiently large so that the self-gravity torque overcomes the tidal torque from the central star. Our analysis and quantitative results can be used to constrain the parameters of transiting circumplanetary disks that may be detected in the future.

Key words: planets and satellites: dynamical evolution and stability - planets and satellites: detection - planets and satellites: rings - planet-disk interactions

1 INTRODUCTION

The age is nearing when direct observations of circumplanetary disks and rings become a reality through photometry. A number of studies have investigated the detectability and observational signatures of circumplanetary disks/rings (Barnes & Fortney 2004; Ohta et al. 2009; Schlichting & Chang 2011; Tusnski & Valio 2011; Zuluaga et al. 2015). Although observational searches for exo-rings have been carried out, most are inconclusive (Brown et al. 2001; Heising et al. 2015; Santos et al. 2015). These searches focused on hot Jupiters, which have Hill radii $r_H \equiv a(M_{\rm p}/3M_*)^{1/3}$ (where a is the planetary semi-major axis, $M_{\rm p}$ is the planet mass, and M_* is the mass of the host star) comparable to their planetary radii $R_{\rm p}$. For this reason, these circumplanetary disks could not have outer radii $r_{\rm out}$ significantly larger than their respective planetary radii.

Mamajek et al. (2012) discovered that the light curve of a young (~ 16 Myr) K5 star 1 SWASP J140747-354542 (hereafter J1407) exhibited a complex series of eclipses that lasted 56 days around the month of April 2007. The central deep (> 3 mag) eclipse was surrounded by two pairs of 1 mag

eclipses occuring at ±12 and ±26 days. They proposed that these eclipses where caused by a large ring system orbiting an unseen companion J1407b (see also van Werkhoven et al. 2014). Other explanations were considered but deemed unlikely. Follow-up observations by Kenworthy et al. (2015) constrain the companion mass to $< 80\,M_{\rm J}$ (where $M_{\rm J}$ is the mass of Jupiter) and semi-major axis (for circular orbits) to $a \simeq 2.2 - 5.6\,{\rm AU}$ (3σ significance). Thus, J1407b is most likely a giant planet or brown dwarf in a 3.5-14 year orbit around the primary star. Modeling the eclipse light curve with a series of inclined, circular optically thick rings gave a best fit outer disk radius of $\sim 0.6\,{\rm AU}$, a significant fraction of the companion's Hill radius (van Werkhoven et al. 2014; Kenworthy & Mamajek 2015). The disk/ring system also contains gaps, which may be cleared by exomoons orbiting around J1407b.

Currently, the ring/disk interpretation of the J1407 light curve remains uncertain, although no serious alternatives have been explored in detail. The ring/disk interpretation can be tested in the coming years if another eclipse event is detected, while a non-detection would put the model under increasing strain. In any case, the possible existence of such a ring system naturally raises questions about the formation of inclined, extended disks/rings around giant plan-

* Email: jjz54@cornell.edu

ets and brown dwarfs. In order to produce a transiting signature, the disk/ring must be inclined with respect to the orbital plane. How are such inclinations produced and maintained?

For giant planets, the inclination of the disk/ring may be tied to the obliquity of the planet due to its rotation-induced quadrupole. The obliquity may be excited through secular spin-orbit resonances, as in the case of Saturn (Hamilton & Ward 2004; Ward & Hamilton 2004; Vokrouhlický & Nesvorný 2015), or through impacts with planetesimals of sufficiently large masses (Lissauer & Safronov 1991). In the case of brown dwarfs, which are thought to form independently of the primary, the disk could be "primordially" misaligned with respect to the binary orbit because of the turbulent motion of gas in the star forming environment (Bate 2009; Bate et al. 2010; Tokuda et al. 2014).

In this paper, we will address the following question: Under what conditions can an extended disk/ring around a planet or brown dwarf maintain its inclination with respect to the planet's orbit in order to exhibit a transit signature? As discussed in Section 2, even when the disk is safely confined within the planet's Hill sphere, the outer region of the disk can still suffer significant tidal torque from the host star. This tidal torque tends to induce differential precession of the disk. Without any internal forces, the disk will lose coherence in shape and inclination. In the presence of dissipation, the disk may reach a equilibrium warp profile (called "Laplace surface") in which the outer region of the disk [beyond the Laplace radius; see Eq. (3) below] becomes aligned with the orbital plane.

In gaseous disks, hydrodynamic forces work to keep the disk coherent, through bending waves (Ivanov & Illarionov 1997; Papaloizou & Lin 1995; Lubow & Ogilvie 2000) or viscosity (Papaloizou & Pringle 1983; Ogilvie 1999). But the rapid variability in the photometric data for the inferred ring system around J1407b implies that the disk/ring system is quite thin, with a ratio of the scaleheight to radius of order $H/r \sim 10^{-3}$ (van Werkhoven et al. 2014), with significant gaps in the disk (Mamajek et al. 2012; Kenworthy & Mamajek 2015).

It is unlikely that hydrodynamical forces are sufficiently strong to maintain the disk's coherence (see Section 5.2).

Another plausible internal torque is self-gravity (e.g., Ward 1981; Touma et al. 2009; Ulubay-Siddiki et al 2009). This is the possibility we will focus on in this paper. Of particular relevance is the work by Ward (1981), who studied the warping of a massive self-gravitating disk in an attempt to explain the inclination of Iapetus, Saturn's moon, with respect to the local Laplace surface. He found that self-gravity of the circumplanetary disk which formed Saturn's satellites could significantly modify the equilibrium inclination/warp profile.

In this paper, we re-examine the warp dynamics of self-gravitating circumplanetary disks in light of the possible detection extended transiting disks. We consider general (possibly large) planetary obliquities, and study both equilibrium disk warp and its time evolution. Our goal is to derive the conditions (in terms of disk mass and density profile) under which an extended circumplanetary disk/ring maintain its inclination with respect to the planet's orbit. In Section 3, we study the equilibrium inclination/warp profile of

the disk, which we will call the *Generalized Laplace Surface*, under the influences of torques from the oblate planet, the distant host star, and disk self-gravity. We show that if the disk is sufficiently massive, the outer region of the disk can maintain significant inclination relative to the planet's orbit. In Section 4, we study the time evolution of disk warp, including the stability of the generalized Laplace surfaces, and the condition required for the disk to be capable of precessing coherently. We summarize our results and discuss their implications in Section 5

Although it is unknown if the object J1407b is a planet or brown dwarf, we will refer to J1407b as a "planet" throughout the rest of the paper.

2   EXTERNAL TORQUES AND THE LAPLACE SURFACE

Consider a planet (mass M_p) in a circular orbit around a central star (mass M_*) with orbital semi-major axis a. We denote the unit orbital angular momentum vector by $\hat{\boldsymbol{l}}_p$. We take the circumplanetary disk to extend from radius $r = r_{in}$ to $r = r_{out}$, as measured from the center of the planet. We assume that the disk is circular. In general, the angular momentum unit vector at each annulus of the disk is a function of radius and time, and is specified by $\hat{\boldsymbol{l}} = \hat{\boldsymbol{l}}(r, t)$.

The circumplanetary disk experiences two external torques, from the host star and from the planet's quadrupole. Averaging over the orbit of the planet, to leading order in the ratio r/a, the tidal torque per unit mass from the star exerted on a disk annulus with unit angular momentum $\hat{\boldsymbol{l}}$ is

$$\boldsymbol{T}_* = \frac{3GM_* r^2}{4a^3} \left(\hat{\boldsymbol{l}} \cdot \hat{\boldsymbol{l}}_p \right) \left(\hat{\boldsymbol{l}} \times \hat{\boldsymbol{l}}_p \right). \tag{1}$$

The quadrupole moment of the planet is related to its J_2 parameter by $I_3 - I_1 = J_2 M_p R_p^2$, where R_p is the radius of the planet, and J_2 depends on the planet's rotation rate Ω_p via $J_2 = (k_2/3)(\Omega_p^2 R_p^3 / GM_p)$. The Love number k_2 is of order 0.4 for giant planets. The torque from the spinning planet on the disk annulus is

$$\boldsymbol{T}_{sp} = \frac{3GM_p R_p^2 J_2}{2r^3} \left(\hat{\boldsymbol{l}} \cdot \hat{\boldsymbol{s}}_p \right) \left(\hat{\boldsymbol{l}} \times \hat{\boldsymbol{s}}_p \right), \tag{2}$$

where $\hat{\boldsymbol{s}}_p$ is the unit vector along the planet's spin axis.

In general, when $\hat{\boldsymbol{l}}$, $\hat{\boldsymbol{l}}_p$, and $\hat{\boldsymbol{s}}_p$ are not parallel to each other, $|\boldsymbol{T}_*|$ dominates at large r while $|\boldsymbol{T}_{sp}|$ dominates at small r. The radius where $|\boldsymbol{T}_*| \sim |\boldsymbol{T}_{sp}|$ defines the Laplace radius

$$r_L \equiv \left(2J_2 \frac{M_p}{M_*} R_p^2 a^3 \right)^{1/5} = \left(6J_2 R_p^2 r_H^3 \right)^{1/5}, \tag{3}$$

where $r_H \equiv a(M_p/3M_*)^{1/3}$ is the Hill radius (Tremaine et al. 2009). Tidal truncation and dynamical stability require that the outer radius of the disk be less than a fraction of r_H, i.e. $\xi \equiv r_{out}/r_H \lesssim 0.4$ (e.g. Quillen & Trilling 1998; Ayliffe & Bate 2009a; Martin & Lubow 2011; Lehébel & Tiscareno 2015). Thus

the ratio of r_L to r_{out} is given by

$$
\frac{r_L}{r_{out}} = \left(\frac{6 J_2 R_p^2}{\xi^3 r_{out}^2} \right)^{1/5}
$$

$$
= 0.18 \left(\frac{J_2}{10^{-2}} \right)^{1/5} \left(\frac{r_{out}}{0.2 r_H} \right)^{-3/5}
$$

$$
\times \left(\frac{R_p}{R_{Jup}} \right)^{2/5} \left(\frac{r_{out}}{0.1 \, AU} \right)^{-2/5}. \tag{4}
$$

where we have scaled J_2 to the value appropriate to gas giants in our Solar System, and r_{out} appropriate to the claimed ring system in J1407 (van Werkhoven et al. 2014).

In the presence of dissipation in the disk, we may expect $\hat{l}(r, t)$ to evolve toward the equilibrium state, in which

$$
\boldsymbol{T}_* + \boldsymbol{T}_{sp} = 0. \tag{5}
$$

The equilibrium orientation of the disk $\hat{l}(r)$, which defines the Lapace surface (Laplace 1805; Tremaine et al. 2009), lies in the plane spanned by the vectors $\hat{\boldsymbol{s}}_p$ and $\hat{\boldsymbol{l}}_p$. Throughout this paper, we assume that the planet's spin angular momentum is much larger than the disk angular momentum, so that $\hat{\boldsymbol{s}}_p$ is fixed in time. Let β_p be the planetary obliquity (the angle between $\hat{\boldsymbol{s}}_p$ and $\hat{\boldsymbol{l}}_p$) and $\beta(r)$ be the warp angle of the disk [the angle between $\hat{\boldsymbol{l}}(r)$ and $\hat{\boldsymbol{l}}_p$]. Equation (5) may be reduced to

$$
0 = z^2 \cos \beta(z) \sin \beta(z)
$$

$$
+ \frac{z_L^5}{z^3} \cos \left[\beta(z) - \beta_p \right] \sin \left[\beta(z) - \beta_p \right], \tag{6}
$$

where we have defined the dimensionless Laplace radius z_L and radial coordinate z by

$$
z_L \equiv r_L / r_{out}, \quad z \equiv r / r_{out}. \tag{7}
$$

Figure 1 depicts the solutions to Eq. (6) for $\beta_p = 30°, 60°$ and $z_L = 0.2, 0.5$. Clearly, in the absence of any internal torque, the outer region of the disk (beyond $\sim 2r_L$) is highly aligned with the planetary orbit, with

$$
\beta(r) \simeq \left(\frac{r_L}{r} \right)^5 \cos \beta_p \sin \beta_p. \tag{8}
$$

Such an aligned outer disk would not produce the transit signal claimed in the J1407 system. To maintain significant inclination in the outer disk, some internal torques are needed. We consider the effect of self-gravity in the next section.

3 GENERALIZED LAPLACE SURFACE: EQUILIBRIUM WITH SELF-GRAVITY

In this section, we consider the influence of self-gravity on the equilibrium warp profile $\hat{l}(r)$ of the disk. Let the surface density of the disk be $\Sigma = \Sigma(r)$. The torque acting on the disk due to its own self-gravity is approximately given by

$$
\boldsymbol{T}_{sg} \simeq \frac{\pi G}{2} \int_{r_{in}}^{r_{out}} dr' \frac{r' \Sigma(r')}{\max(r, r')} \chi b_{3/2}^{(1)}(\chi)
$$

$$
\times \left[\hat{\boldsymbol{l}}(r) \cdot \hat{\boldsymbol{l}}(r') \right] \left[\hat{\boldsymbol{l}}(r) \times \hat{\boldsymbol{l}}(r') \right], \tag{9}
$$

where $\chi = \min(r, r') / \max(r, r')$ and $b_{3/2}^{(1)}(\chi)$ is the Laplace coefficient

$$
b_{3/2}^{(1)}(\chi) = \frac{2}{\pi} \int_0^{\pi} \frac{\cos \theta d\theta}{(1 - 2\chi \cos \theta + \chi^2)^{3/2}}. \tag{10}
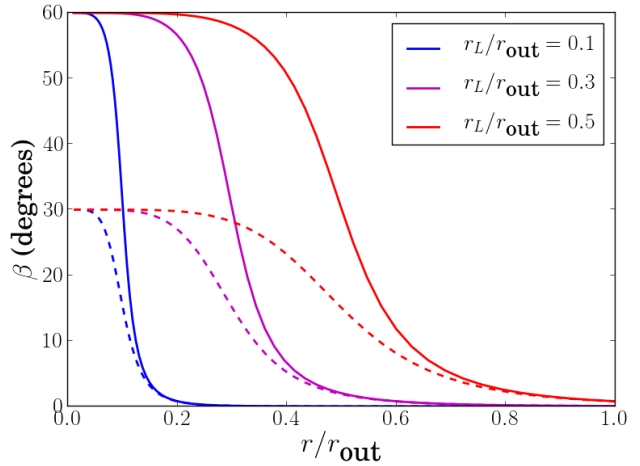$$

Figure 1. Equilibrium disk inclination profile (Laplace surface without self-gravity). The quantity β is the angle between $\hat{l}$ and $\hat{l}_p$. The different lines are for $r_L/r_{out} = 0.1$ (blue), 0.3 (magenta) and 0.5 (red). The planetary obliquity β_p is assumed to be 60° (solid lines) and 30° (dotted lines).

Eq. (9) is an approximation which recovers two limits: When $|\hat{l}(r) \times \hat{l}(r')| \ll 1$, it reduces to Eq. (8) of Tremaine (1991) and Eq. (47) of Tremaine & Davis (2014); when $\chi \ll 1$, $b_{3/2}^{(1)}(\chi) \simeq 3\chi$ (Murray & Dermott 1999) and we recover the quadrupole approximation:

$$
\boldsymbol{T}_{sg} \simeq \frac{3\pi G}{2} \int_{r_{in}}^{r_{out}} dr' \frac{r' \Sigma(r')}{\max(r, r')} \chi^2
$$

$$
\times \left[\hat{\boldsymbol{l}}(r) \cdot \hat{\boldsymbol{l}}(r') \right] \left[\hat{\boldsymbol{l}}(r) \times \hat{\boldsymbol{l}}(r') \right]. \tag{11}
$$

The integrand of Eq. (9) becomes invalid when $\chi \sim 1$ and $|\hat{l}(r) \times \hat{l}(r')| \sim 1$ (i.e., when two close-by annuli have a large mutual inclination), and a different formalism is needed to calculate the torque acting on a disk from its own self-gravity (e.g. Kuijken 1991; Arnaboldi & Sparke 1994; Ulubay-Siddiki et al. 2009). In the appendix, we review the exact equations for calculating internal self-gravity torques for arbitrary χ and $|\hat{l}(r) \times \hat{l}(r')|$. Our numerical calculations based on these exact (but much more complicated) equations show that they provide only minor quantitative corrections to the disk warp profile and the inclination at the outer disk radius. For this reason, we will use the much simpler approximation (9) for the remainder of this paper.

For concreteness, we consider a power-law surface density profile

$$
\Sigma(r) = \Sigma_{out} \left(\frac{r_{out}}{r} \right)^p. \tag{12}
$$

Then the disk mass is (assuming $r_{in} \ll r_{out}$)

$$
M_d \simeq \frac{2\pi}{2 - p} \Sigma_{out} r_{out}^2, \tag{13}
$$

and the total disk angular momentum is

$$
L_d \simeq \frac{4\pi}{5 - 2p} \Sigma_{out} r_{out}^2 \sqrt{G M_p r_{out}}. \tag{14}
$$

It is useful to compare the magnitude of $|\boldsymbol{T}_{sg}|$ to the external torques acting on the disk (see Fig. 2). Ignoring geometrical factors relating to the angles between $\hat{\boldsymbol{l}}, \hat{\boldsymbol{l}}_p$ and
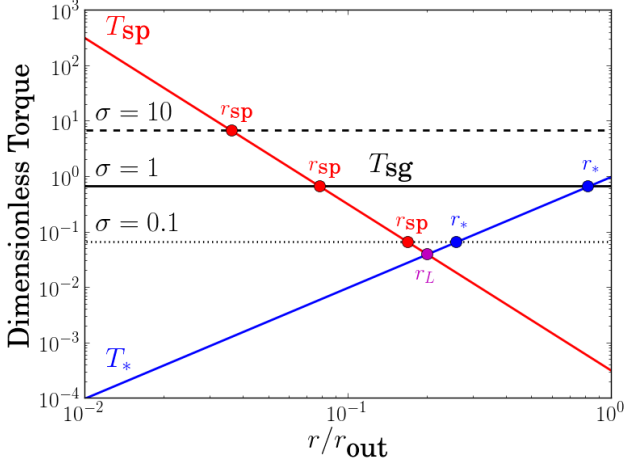
Figure 2. Torques on the disk based on the estimates (15)-(17) and normalized by $|\boldsymbol{T}_*(r_{\text{out}})|$. The tidal torque from the star ($\boldsymbol{T}_*$) is in blue, and the torque from the spinning planet ($\boldsymbol{T}_{\text{sp}}$) is in red. The torque from self-gravity ($\boldsymbol{T}_{\text{sg}}$) is in black, with three values of σ [see Eq. (20)] as indicated, all for $p = 1$ [see Eq. (12)]. The three critical radii in the disk (r_{sp}, r_L, r_*) are marked.

$\hat{\boldsymbol{s}}_{\text{p}}$, we have to an order of magnitude [see Eqs. (9), (1), and (2)]

$$|\boldsymbol{T}_{\text{sg}}| \sim \pi G \Sigma(r) r \qquad (15)$$

$$|\boldsymbol{T}_*| \sim \frac{3 G M_* r^2}{4 a^3} \qquad (16)$$

$$|\boldsymbol{T}_{\text{sp}}| \sim \frac{3 G M_{\text{p}} R_{\text{p}}^2 J_2}{2 r^3}. \qquad (17)$$

Thus

$$\frac{|\boldsymbol{T}_{\text{sg}}|}{|\boldsymbol{T}_*|} \sim \frac{2(2-p)}{3} \sigma \left(\frac{r_{\text{out}}}{r} \right)^{1+p} \equiv \left(\frac{r_*}{r} \right)^{1+p}, \qquad (18)$$

$$\frac{|\boldsymbol{T}_{\text{sg}}|}{|\boldsymbol{T}_{\text{sp}}|} \sim \frac{2(2-p)}{3} \frac{\sigma}{z_L^5} \left(\frac{r}{r_{\text{out}}} \right)^{4-p} \equiv \left(\frac{r}{r_{\text{sp}}} \right)^{4-p}, \qquad (19)$$

where we have defined the dimensionless parameter σ (which measures $|\boldsymbol{T}_{\text{sg}}|/|\boldsymbol{T}_*|$ at $r = r_{\text{out}}$) as

$$\sigma \equiv \frac{M_{\text{d}}}{M_*} \left(\frac{a}{r_{\text{out}}} \right)^3 = 0.38 \left(\frac{r_{\text{out}}}{0.2\, r_H} \right)^{-3} \left(\frac{M_{\text{d}}}{10^{-3} M_{\text{p}}} \right). \quad (20)$$

In Eqs. (18) and (19), r_* and r_{sp} are set by $|\boldsymbol{T}_{\text{sg}}|/|\boldsymbol{T}_*| \sim 1$ and $|\boldsymbol{T}_{\text{sg}}|/|\boldsymbol{T}_{\text{sp}}| \sim 1$ respectively. Recall the Laplace radius r_L is set by $|\boldsymbol{T}_*| \sim |\boldsymbol{T}_{\text{sp}}|$. For radii $r \lesssim r_{\text{sp}}$, $\boldsymbol{T}_{\text{sp}}$ dominates and the disk annuli tend to be aligned with the planetary spin axis. For $r \gtrsim r_*$, $\boldsymbol{T}_*$ dominates and the disk tends to be aligned with the planet's orbit. For $r_{\text{sp}} \lesssim r \lesssim r_*$, $\boldsymbol{T}_{\text{sg}}$ dominates and self-gravity strongly influences the disk warp profile.

The equilibrium disk warp profile $\hat{\boldsymbol{l}}(r)$ including the effect of self-gravity is determined by the equation

$$\boldsymbol{T}_* + \boldsymbol{T}_{\text{sp}} + \boldsymbol{T}_{\text{sg}} = 0. \qquad (21)$$

With $\hat{\boldsymbol{l}}(r)$ lying in the plane spanned by $\hat{\boldsymbol{l}}_{\text{p}}$ and $\hat{\boldsymbol{s}}_{\text{p}}$, this
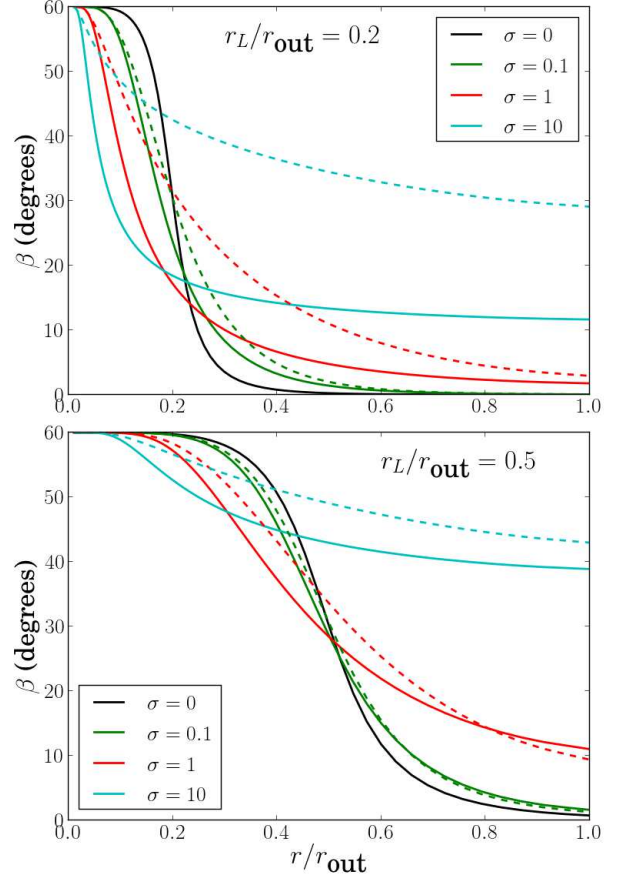

Figure 3. Equilibrium disk inclination profile $\beta(r)$ including the effect of self gravity (the generalized Laplace surface), for different values of r_L/r_{out} and σ [see Eq. (20)] as indicated. The planetary obliquity is assumed to be $\beta_{\text{p}} = 60°$. The $\sigma = 0$ curves correspond to the standard Laplace surface (without self-gravity). The solid lines are for the surface density power-law index $p = 1$, and dashed lines for $p = 1.5$.

reduces to

$$0 = z^2 \cos \beta(z) \sin \beta(z)$$
$$+ \frac{z_L^5}{z^3} \cos \left[\beta(z) - \beta_{\text{p}} \right] \sin \left[\beta(z) - \beta_{\text{p}} \right]$$
$$+ \frac{2-p}{3} \sigma \int_{r_{\text{in}}/r_{\text{out}}}^1 \text{d}z' \frac{(z')^{1-p}}{\max(z, z')} \chi b_{3/2}^{(1)}(\chi)$$
$$\times \cos \left[\beta(z) - \beta(z') \right] \sin \left[\beta(z) - \beta(z') \right]. \quad (22)$$

Figure 3 depicts a sample of the equilibrium disk inclination profile $\beta(r)$ for $r_L/r_{\text{out}} = 0.2, 0.5$ and $p = 1, 1.5$, with various values of the disk mass parameter σ. As expected, for sufficiently large σ, self-gravity can significantly increase the outer disk's inclination.

Figure 4 shows the outer disk inclination angle $\beta(r_{\text{out}})$ as a function of σ. Decreasing the parameter p or r_L/r_{out} results in a decrease of $\beta(r_{\text{out}})$. This can be understood as follows: The disk inside r_L is roughly aligned with the planet's spin. This inner disk, together with the planet's intrinsic quadrupole, act on the outer disk to resist the tidal torque from the host star and generate $\beta(r_{\text{out}})$. Reducing p leads to a smaller effective quadrupole of the inner disk, and therefore yielding a smaller $\beta(r_{\text{out}})$.
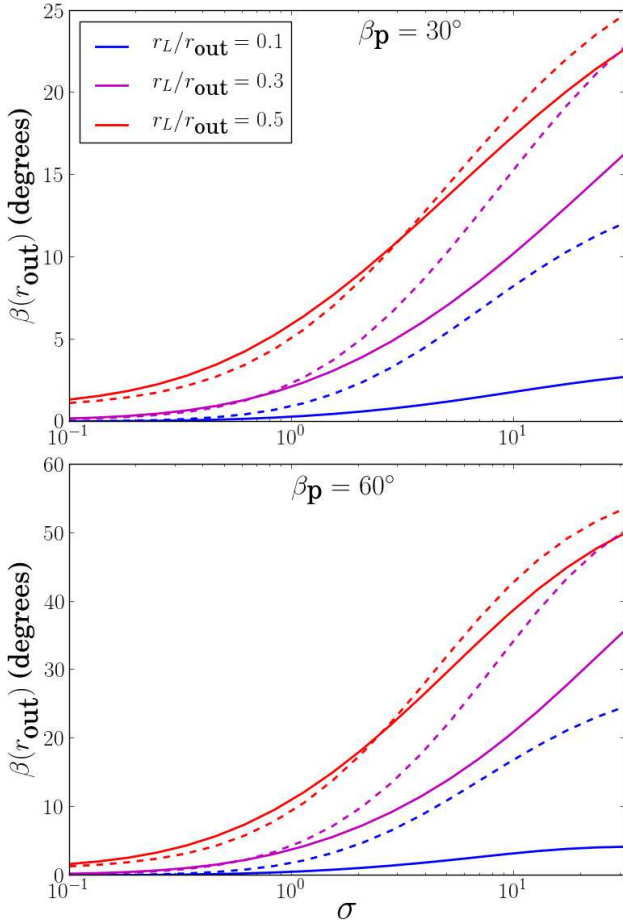
Figure 4. Equilibrium inclination of the disk at the outer radius [the angle between $\hat{\boldsymbol{l}}(r_{\rm out})$ and $\hat{\boldsymbol{l}}_{\rm p}$], as a function of the disk mass parameter σ [see Eq.(20)]. The top panel is for the planetary obliquity $\beta_{\rm p} = 30°$, and the lower panel for $\beta_{\rm p} = 60°$. Different colored curves correspond to different values of $r_L/r_{\rm out}$ as indicated. The solid lines are for the surface density profile of $p = 1$, while the dashed lines are for $p = 1.5$.

The qualitative behavior of Fig. 4 at low σ may be understood analytically. For $\beta(r_{\rm out}) \ll \beta_p$, we use the approximate solution $\beta(r) \sim \beta_{\rm p}\Theta[(r/r_{\rm out}) - (r_L/r_{\rm out})]$ in the integrand of Eq. (22) (Θ is the Heavyside step function). We find, to an order of magnitude,

$$\beta(r_{\rm out}) \sim \left[\left(\frac{r_L}{r_{\rm out}} \right)^5 + \left(\frac{2-p}{4-p} \right) \sigma \left(\frac{r_L}{r_{\rm out}} \right)^{4-p} \right]$$
$$\times \cos\beta_{\rm p} \sin\beta_{\rm p}. \quad (23)$$

Comparing to Eq. (8), the second term in Eq. (23) may be understood as the correction to the planet's effective quadrupole due to inner disk's self-gravity. We see that in order to achieve significant $\beta(r_{\rm out})$, both σ and $r_L/r_{\rm out}$ must be sufficiently large. We note that while Eq. (23) captures the correct trend of how $\beta(r_{\rm out})$ depends on σ, $r_L/r_{\rm out}$ and p, it is necessary to solve Eq. (22) to obtain the quantitatively accurate result depicted in Fig. 4.

4 TIME EVOLUTION OF DISK WARP

In this Section, we first use numerical integrations to examine the stability property of the generalized Laplace Surfaces obtained in Section 3. We then consider the possibility of coherent precession of warped self-gravitating disks.

4.1 Stability of Generalized Laplace Equilibria

In Tremaine et al. (2009), it was found that the solutions to Eq. (5) (without disk self-gravity) were unstable when $\beta_{\rm p} > 90°$. Although in this paper we only consider disk warp profiles with $\beta_{\rm p} < 90°$, it is not immediately obvious if the addition of self-gravity changes the stability of the generalized Laplace surfaces obtained by solving Eq. (21). A complete analysis of the Laplace equilibria [which we denote by $\hat{\boldsymbol{l}}_0(r)$] would require one to find the full eigenvalue spectrum of the perturbed equation of motion for $\hat{\boldsymbol{l}}(r, t)$. We do not carry out such an analysis here. Instead, we use numerical integrations to examine how a small deviation of $\hat{\boldsymbol{l}}(r, t)$ from $\hat{\boldsymbol{l}}_0(r)$ evolves in time.

The evolution equation for the disk warp profile $\hat{\boldsymbol{l}}(r, t)$ is

$$r^2\Omega\frac{\partial\hat{\boldsymbol{l}}}{\partial t} = \boldsymbol{T}_* + \boldsymbol{T}_{\rm sp} + \boldsymbol{T}_{\rm sg}, \quad (24)$$

where $\Omega(r) = \sqrt{GM_{\rm p}/r^3}$. The small perturbation $\boldsymbol{j} \equiv \hat{\boldsymbol{l}}(r, t) - \hat{\boldsymbol{l}}_0(r)$ satisfies

$$r^2\Omega\frac{\partial\boldsymbol{j}}{\partial t} = \boldsymbol{T}_* + \boldsymbol{T}_{\rm sp} + \boldsymbol{T}_{\rm sg}. \quad (25)$$

We consider two indepedent initial perturbations:

$$\boldsymbol{j}(r, t = 0) = 0.02 \sin\left[\frac{\pi(r - r_{\rm in})}{r_{\rm out} - r_{\rm in}} \right] \left(\frac{\hat{\boldsymbol{s}}_{\rm p} \times \hat{\boldsymbol{l}}_{\rm p}}{|\hat{\boldsymbol{s}}_{\rm p} \times \hat{\boldsymbol{l}}_{\rm p}|} \right) \quad (26)$$

and

$$\boldsymbol{j}(r, t = 0) = 0.02 \sin\left[\frac{\pi(r - r_{\rm in})}{r_{\rm out} - r_{\rm in}} \right] \left(\frac{\hat{\boldsymbol{l}}_0 \times (\hat{\boldsymbol{s}}_{\rm p} \times \hat{\boldsymbol{l}}_{\rm p})}{|\hat{\boldsymbol{l}}_0 \times (\hat{\boldsymbol{s}}_{\rm p} \times \hat{\boldsymbol{l}}_{\rm p})|} \right). \quad (27)$$

Equation (26) corresponds to a perturbation perpendicular to the plane spanned by the Laplace surface, while Eq. (27) corresponds to a slight change in the disk inclination profile $\beta(r)$. We choose the r-dependence in Eqs. (26) and (27) such that $\boldsymbol{j} = 0$ at $r = r_{\rm in}$ and $r = r_{\rm out}$.

Figure 5 shows some examples of our numerical integration results. We define the quantity

$$j_{\rm max}(t) \equiv \max_{r \in [r_{\rm in}, r_{\rm out}]}(|\boldsymbol{j}(r, t)|), \quad (28)$$

and plot $j_{\rm max}$ for the initial conditions (26) and (27), with parameters $\beta_{\rm p} = 30°, 60°$ and $\sigma = 0.1, 10$. We see that $j_{\rm max}$ is bounded in all cases. We have carried out calculations for other initial conditions and found similar behaviors for $j_{\rm max}$. We conclude that the equilibrium profile $\hat{\boldsymbol{l}}_0(r)$ are stable (for $\beta_{\rm p} < 90°$).

In addition to the inclination instability, it was shown in Tremaine et al. (2009) that the Laplace surface (without self-gravity) is unstable to eccentricity growth when $\beta_{\rm p} \gtrsim 69°$. This "eccentricity instability" cannot be probed by our analysis, and is beyond the scope of this paper. All examples considered in this paper have planetary obliquities less than this critical angle.
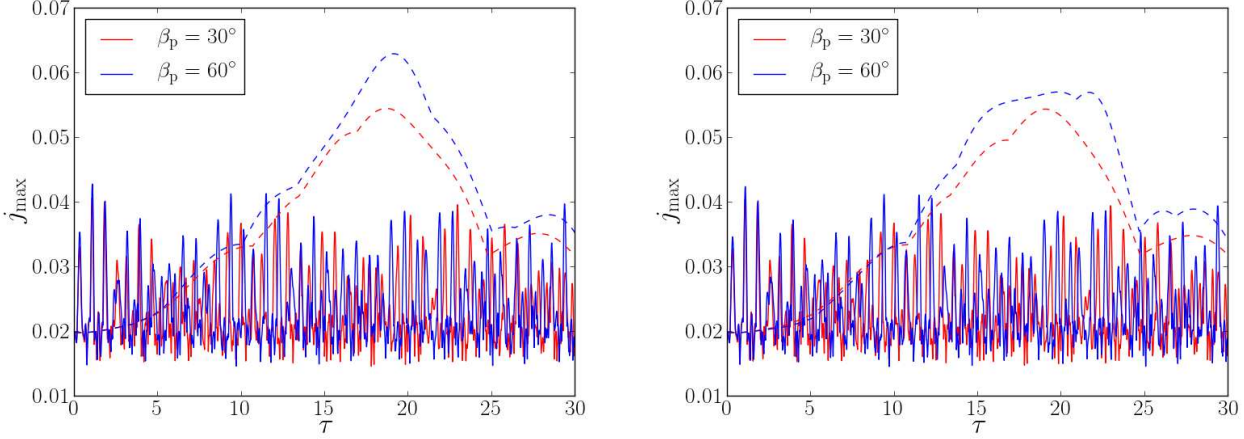
Figure 5. Time evolution of the quantity $j_{\max}$ [Eq. (28)], with the initial condition given by (26) (left panel) and (27) (right panel). Solid lines denote $\sigma = 10$, dotted lines denote $\sigma = 0.1$. Values of β_{p} are as indicated.

4.2 Coherent Disk Precession

The generalized Laplace surfaces studied in Section 3 correspond to the disk warp equilibria that may be attained when the disk experiences sufficient internal dissipation. However, we could also imagine situations in which circumplanetary disks are formed with a warp profile that is "out of equilibrium". It is of interest to consider the time evolution of such "out-of-equilibrium" disks. In particular, we are interested in the following scenario/question: if a disk is formed with a large inclination at r_{out} with respect to the planet's orbit, under what condition can the disk maintain its coherence and large inclination at r_{out}?

In general, the disk warp profile $\hat{\boldsymbol{l}}(r, t)$ evolves according to Eq. (24). Without self-gravity, the disk will develop large incoherent warps and twists due to strong differential torques, and may eventually break. With sufficient self-gravity, coherent precession of the disk may be possible.

For concreteness, we consider an initially flat disk with $\hat{\boldsymbol{l}}$ aligned with the planet's spin axis $\hat{\boldsymbol{s}}_{\mathrm{p}}$. Both $\hat{\boldsymbol{s}}_{\mathrm{p}}$ and $\hat{\boldsymbol{l}}_{\mathrm{p}}$ are assumed to be fixed in time, since the planet's spin and orbital angular momenta are much larger than the disk angular momentum. To determine the evolution of the disk warp profile, we divide the disk into 30 rings spaced logarithmically in radius, with r_i ($i = 1, 2, \ldots, 30$) ranging from $5 \times 10^{-2} r_{\mathrm{out}}$ to r_{out}. We then integrate Eq. (24) to evolve the orientation of the individual ring $\hat{\boldsymbol{l}}(r_i, t)$.

Figures 6 and 7 show a sample numerical result, for integration time up to $\tau = t\omega_*(r_{\mathrm{out}}) = 30$, where

$$\omega_*(r_{\mathrm{out}}) = \frac{3GM_*}{4a^3\Omega(r_{\mathrm{out}})} \tag{29}$$

is the (approximate) precession frequency of the outer disk annulus torqued by the central star. The planetary obliquity is fixed at $\beta_{\mathrm{p}} = 40°$, with $p = 1$ and $r_L/r_{\mathrm{out}} = 0.2$. We consider three values of σ: 10, 1 and 0.1. In addition to the disk inclination angle $\beta(r, t)$ [the angle between $\hat{\boldsymbol{l}}(r, t)$ and $\hat{\boldsymbol{l}}_{\mathrm{p}}$], we also show the disk twist angle $\phi(r, t)$ [the angle between $\hat{\boldsymbol{l}}_{\mathrm{p}} \times \hat{\boldsymbol{l}}(r, t)$ and $\hat{\boldsymbol{l}}_{\mathrm{p}} \times \hat{\boldsymbol{s}}_{\mathrm{p}}$]. In all three cases, when $r \lesssim r_{\mathrm{sp}}$ the disk annuli remain mostly aligned with the planetary spin, with $\beta \approx \beta_{\mathrm{p}} = 40°$. For the $\sigma = 10$ case, the region of the disk beyond r_{sp} precesses coherently, while for the

low-mass case ($\sigma = 0.1$), the disk's self-gravity is not able to enforce coherence, since different disk annuli precess at different rates. This transition of the coherent behavior occurs at $r_\star \sim r_{\mathrm{out}}$, or equivalently $\sigma \sim 1$. From Eq. (18) we have

$$\frac{r_\star}{r_{\mathrm{out}}} = \left[\frac{2(2-p)}{3}\sigma\right]^{1/(1+p)}. \tag{30}$$

Thus, coherent precession of the outer disk requires $\sigma \gtrsim 1$, or in terms of disk mass,

$$M_{\mathrm{d}} \gtrsim 2.67 \times 10^{-3} M_{\mathrm{p}} \left(\frac{r_{\mathrm{out}}}{0.2\, r_H}\right)^3. \tag{31}$$

When the disk mass is high ($\sigma \gg 1$), the dynamical behavior is relatively simple. This may be understood with the model put forth in the next section.

4.3 Model for high σ disk

We assume that for radii $r < r_{\mathrm{sp}}$, the disk annuli stay aligned with the oblate planet, while for $r \geq r_{\mathrm{sp}}$ the disk is a rigid plate being torqued externally by the star and the oblate planet [see Eqs. (1) and (2)]. In other words, we model the disk inclination profile as

$$\hat{\boldsymbol{l}}(r, t) = \left\{ \begin{array}{ll} \hat{\boldsymbol{s}}_{\mathrm{p}} & r < r_{\mathrm{sp}} \\ \hat{\boldsymbol{n}}(t) & r \geq r_{\mathrm{sp}} \end{array} \right., \tag{32}$$

with $\hat{\boldsymbol{n}}$ evolving in time according to

$$\frac{d\hat{\boldsymbol{n}}}{dt} = \bar{\omega}_*(\hat{\boldsymbol{n}}\cdot\hat{\boldsymbol{l}}_{\mathrm{p}})(\hat{\boldsymbol{l}}_{\mathrm{p}}\times\hat{\boldsymbol{n}}) + (\bar{\omega}_{\mathrm{sp}} + \bar{\omega}_{\mathrm{d,in}})(\hat{\boldsymbol{n}}\cdot\hat{\boldsymbol{s}}_{\mathrm{p}})(\hat{\boldsymbol{s}}_{\mathrm{p}}\times\hat{\boldsymbol{n}}), \tag{33}$$

where

$$\bar{\omega}_* = \frac{2\pi}{L_{\mathrm{d,out}}} \int_{r_{\mathrm{sp}}}^{r_{\mathrm{out}}} \Sigma(r) r \left(\frac{3GM_* r^2}{4a^3}\right) dr, \tag{34}$$

$$\bar{\omega}_{\mathrm{sp}} = \frac{2\pi}{L_{\mathrm{d,out}}} \int_{r_{\mathrm{sp}}}^{r_{\mathrm{out}}} \Sigma(r) r \left(\frac{3GM_{\mathrm{p}} R_{\mathrm{p}}^2 J_2}{2r^3}\right) dr, \tag{35}$$

$$\bar{\omega}_{\mathrm{d,in}} = \frac{2\pi}{L_{\mathrm{d,out}}} \int_{r_{\mathrm{sp}}}^{r_{\mathrm{out}}} \Sigma(r) r \left(\int_{r_{\mathrm{in}}}^{r_{\mathrm{sp}}} \frac{3\pi G \Sigma(r')(r')^3}{2r^3} dr'\right) dr, \tag{36}$$

$$L_{\mathrm{d,out}} = 2\pi \int_{r_{\mathrm{sp}}}^{r_{\mathrm{out}}} \Sigma(r) r^3 \Omega(r) dr. \tag{37}$$
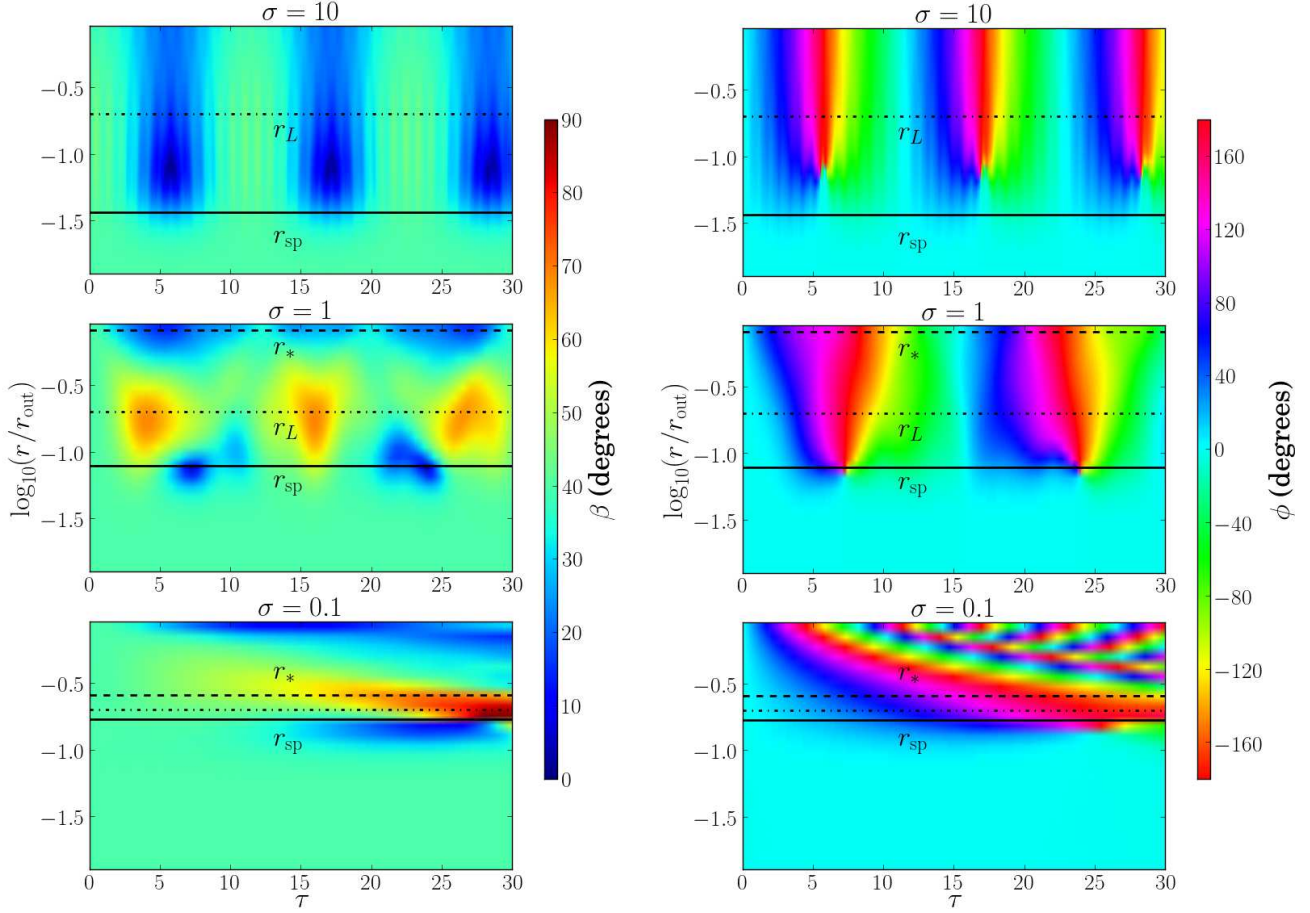
Figure 6. Evolution of the disk inclination $\beta(r,t)$ (left panels) and twist angle $\phi(r,t)$ (right panels) for three different disk mass parameters: $\sigma = 10$ (top), $\sigma = 1$ (middle), and $\sigma = 0.1$ (bottom). The dimensionless time is $\tau = t\omega_*(r_{\rm out})$ [see Eq. (29)]. The horizontal lines mark the locations of $r_{\rm sp}$ (solid), $r_*/r_{\rm out}$ (dashed) and r_L (dot-dashed), to indicate where self-gravity and external torques dominate (see Fig. 2). The planetary obliquity is $\beta_{\rm p} = 40°$ and the Laplace radius is $r_L/r_{\rm out} = 0.2$.

and $\omega_*(r_{\rm out})$ is given by Eq. (29). Note that $r_{\rm sp}$ depends on σ [see Eq. (19) and Fig. 2]. Assuming $r_{\rm in} \ll r_{\rm sp} \ll r_{\rm out}$,

$$\bar{\omega}_* \simeq \omega_*(r_{\rm out})\frac{5-2p}{2(4-p)}, \tag{38}$$

$$\bar{\omega}_{\rm sp} \simeq \omega_*(r_{\rm out})\frac{5-2p}{2(1+p)}\left(\frac{r_L}{r_{\rm out}}\right)^5\left(\frac{r_{\rm out}}{r_{\rm sp}}\right)^{1+p}, \tag{39}$$

$$\bar{\omega}_{\rm d,in} \simeq \omega_*(r_{\rm out})\frac{(5-2p)(2-p)}{2(4-p)(1+p)}\sigma\left(\frac{r_{\rm sp}}{r_{\rm out}}\right)^{3-2p}. \tag{40}$$

In Fig. 8, we show the outer disk inclination β and precession angle ϕ for $\hat{n}$, with $r_L/r_{\rm out} = 0.2$ and $p = 1$. The qualitative behavior seen in Figs. 6 and 7 is reproduced. In particular, for $\sigma = 10$, the outer disk undergoes full precession in ϕ while the inclination β nutates; for $\sigma = 30$, the disk librates in ϕ around $0°$, with β varying between $0°$ and $40°$.

In our model, the behavior of ϕ switches from precession to libration at $\sigma \approx 23$.

5 SUMMARY AND DISCUSSION

5.1 Key Results

Motivated by the recent (tentative) observational evidence for the circumplanetary disk/ring system around the young K5 star 1 SWASP J140747-354542 (Mamajek et al. 2012; van Werkhoven et al. 2014; Kenworthy et al. 2015; Kenworthy & Mamajek 2015), we have presented a general theoretical study of the inclination (warp) profile of extended disks around giant planets (or brown dwarfs). Such a disk experiences torques from the host star and the oblate planet. In the absence of any internal torque, the disk may assume an equilibrium warp profile (the Laplace surface; see Section 2), such that the outer disk beyond the Laplace radius r_L [see Eq. (3)] tends to be aligned with the planet's orbit (see Fig. 1). We have studied how self-gravity of the disk affects the steady-state disk inclination profile (Fig. 3). In general, for a given planetary obliquity $\beta_{\rm p}$, the outer disk inclination can be increased due to the "rigidity" provided by the disk's self-gravity. To produce a non-negligible outer disk misalignment requires that the combination of the disk mass and $r_L/r_{\rm out}$ be sufficiently large [see Fig. 4 and Eq. (23)]. The required disk mass is larger for smaller $r_L/r_{\rm out}$. (Of
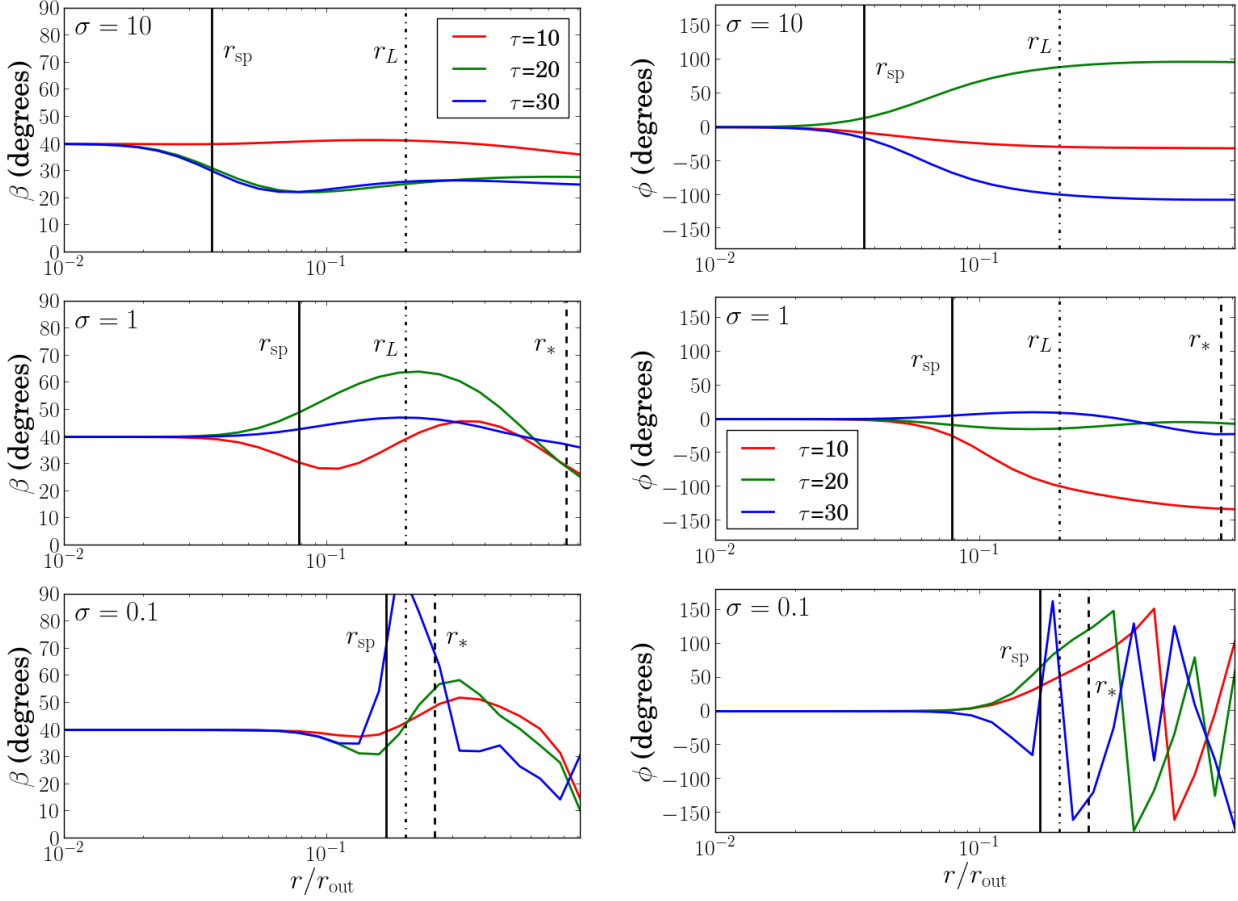
Figure 7. Snapshots of the disk inclination profile $\beta(r,t)$ (left) and twist profile $\phi(r,t)$ (right) at $\tau = 10$ (red), $\tau = 20$ (green) and $\tau = 30$ (blue), for the evolution depicted in Fig. 6. The vertical lines mark the locations $r_{\rm sp}$ (solid), r_* (dashed) and r_L (dot-dashed), indicating where self-gravity and external torques dominate.

course, if the disk lies completely inside r_L, i.e. $r_L/r_{\rm out} \gtrsim 1$, self-gravity is not needed to achieve misalignment of the disk since $\beta \simeq \beta_{\rm p}$.)

We have shown that the generalized Laplace equilibria for disk warp profiles are stable against small inclination perturbations (Section 4.1). Because a circumplanetary disk may not relax to a steady state in the absence of internal dissipation, we have also studied the dynamical evolution of a disk initially aligned with the planet's spin (Section 4.2). Such a disk can attain misalignment with respect to the orbital plane if it can precess coherently and if $\beta_{\rm p} \neq 0$. We showed that to achieve coherent disk precession, the disk's self-gravity must dominate over the influence of the star's tidal torque throughout the disk. This coherence requirement leads to a lower bound on the disk mass [Eq. (31)]:

$$M_{\rm d} \gtrsim 2.67 \times 10^{-3} M_{\rm p} \left(\frac{r_{\rm out}}{0.2\, r_H} \right)^3.$$

Of course, this mass constraint is needed only if $r_{\rm out} > r_L$.

5.2   Hydrodynamical Effects

In this paper we have focused on the effect of self-gravity in maintaining the coherence and inclination of circumplan-

etary disks. Here we briefly comment on hydrodynamical effects internal to the disk.

As noted in Section 1, hydrodynamic forces work to keep the disk coherent through either bending waves or viscosity. If the disk viscosity parameter α satisfies $\alpha \lesssim H/r$, the warp disturbances propagate through the circumplanetary disk in the form of bending waves. In order to enforce coherence, a bending wave must propagate throughout the disk faster than a precession period from the tidal torque of the host star (Larwood et al. 1996). The tidal precession period is of order $t_* \sim 2\pi r^2 \Omega/|\boldsymbol{T}_*| \sim (8\pi/\Omega)(r_H/r)^3$, while the bending-wave crossing time is $t_{\rm bend} \simeq 2r/c_{\rm s} \simeq (2/\Omega)(r/H)$ ($c_{\rm s}$ is the disk sound speed). Thus the small value of H/r ($\sim 10^{-3}$ for the inferred ring system around J1407b) makes t_* smaller than $t_{\rm bend}$ when the disk extends to a significant fraction of the Hill radius.

If the disk viscosity parameter satisfies $\alpha \gtrsim H/r$, hydrodynamical forces communicate through the disk in the form of viscosity. The the internal viscous torque (per unit mass) is (Papaloizou & Pringle 1983)

$$|\boldsymbol{T}_{\rm visc}| = \frac{r^2 \Omega^2}{2} \left(\frac{H}{r} \right) \left(3\alpha + \frac{1}{2\alpha} \left| \frac{\partial \hat{\boldsymbol{l}}}{\partial \ln r} \right| \right) \qquad (41)$$

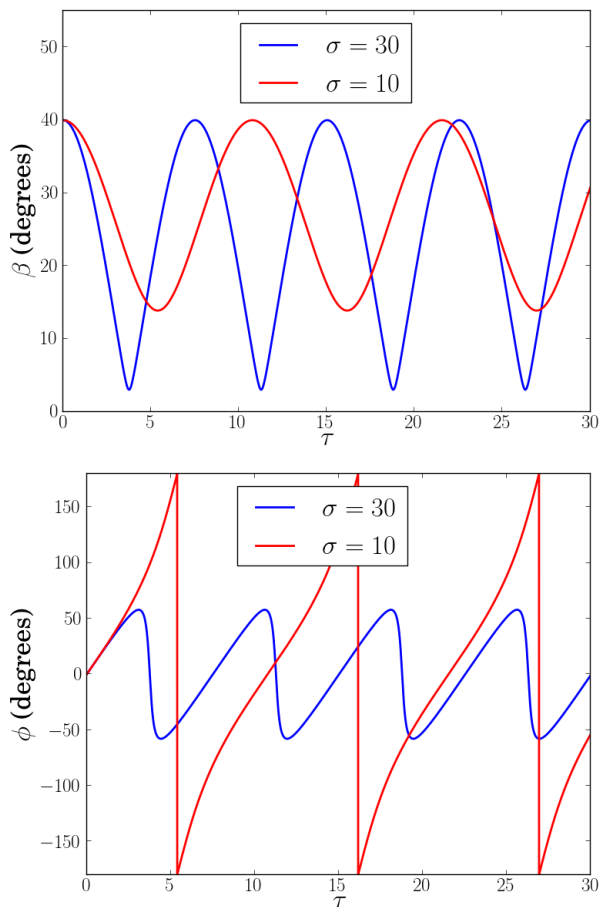Comparing this with the tidal torque $|\boldsymbol{T}_*|$ shows that unless

find

$$Q(r_{\text{out}}) = \frac{c_{\text{s}}(r_{\text{out}})\kappa(r_{\text{out}})}{\pi G\Sigma(r_{\text{out}})}$$

$$\simeq \frac{2}{2-p}\left(\frac{H(r_{\text{out}})}{10^{-3}r_{\text{out}}}\right)\left(\frac{10^{-3}M_{\text{p}}}{M_{\text{d}}}\right). \quad (42)$$

where we have used $c_{\text{s}} \simeq H\Omega$, $\kappa \simeq \Omega \simeq \sqrt{GM_{\text{p}}/r^3}$ (H is the disk scale-height). Requiring $Q \gtrsim 1$ for stability puts an upper limit on M_{d}, and thus the size of the disk. Combining Eqs. (42) and (31), we find

$$\frac{r_{\text{out}}}{r_H} \lesssim 0.35 \left(\frac{H}{10^{-3}r_{\text{out}}}\right)^{1/3}. \quad (43)$$

This puts a strong constraint on the putative ring/disk system around J1407b.

Our work shows that in general, an extended circumplanetary disk is warped when in a steady state or undergoing coherent precession. This warp depends on the Laplace radius [see Eq. (3)] and the disk mass. Direct observations of such a warped circumplanetary disk would constrain the planet's oblateness (the J_2 parameter), complementing photometric constraints (Carter & Winn 2010; Zhu et al. 2014).

Although our work is motivated by the the putative J1407b ring system, our results can be easily adapted to circumplanetary disk/ring systems in general. We expect that the analysis developed in this paper can be a useful tool to evaluate the stability of circumplanetary disk/ring systems detected in the future.

ACKNOWLEDGMENTS

REFERENCES

Arnaboldi, M., & Sparke, L. S. 1994, AJ, 107, 958
Ayliffe, B. A., & Bate, M. R. 2009, MNRAS, 397, 657
Barnes, J. W., & Fortney, J. J. 2004, ApJ, 616, 1193
Bate, M. R. 2009, MNRAS, 392, 590
Bate, M. R., Lodato, G., & Pringle, J. E. 2010, MNRAS, 401, 1505
Brown, T. M., Charbonneau, D., Gilliland, R. L., Noyes, R. W., & Burrows, A. 2001, ApJ, 552, 699
Canup, R. M., & Ward, W. R. 2006, Nature, 441, 834
Carter, J. A., & Winn, J. N. 2010, ApJ, 709, 1219
Doğan, S., Nixon, C., King, A., & Price, D. J. 2015, MNRAS, 449, 1251
Hamilton, D. P., & Ward, W. R. 2004, AJ, 128, 2510
Heising, M. Z., Marcy, G. W., & Schlichting, H. E. 2015, ApJ, 814, 81
Ivanov, P. B., & Illarionov, A. F. 1997, MNRAS, 285, 394
Kenworthy, M. A., Lacour, S., Kraus, A., et al. 2015, MNRAS, 446, 411
Kenworthy, M. A., & Mamajek, E. E. 2015, ApJ, 800, 126
Kuijken, K. 1991, ApJ, 376, 467

Figure 8. Evolution of the (flat) outer disk inclination β and twist angle ϕ for the simple model [see Eqs. (32)-(33)], with two values for the disk mass parameter σ as indicated. For $\sigma = 30$, the disk normal vector $\hat{\boldsymbol{n}}$ precesses around the planetary spin vector $\hat{\boldsymbol{s}}_{\text{p}}$, with ϕ librating around $\phi = 0°$, while β varies from $0°$ to $40°$. For $\sigma = 10$, the outer disk precesses fully around the planetary orbital angular momentum axis $\hat{\boldsymbol{l}}_{\text{p}}$, indicated by ϕ spanning the full range of $-180°$ to $180°$, while β remains more or less constant. The Laplace radius is $r_L/r_{\text{out}} = 0.2$, with $p = 1$.

the disk warp $|\partial\hat{\boldsymbol{l}}/\partial \ln r|$ is significant, the viscous torque will have difficulty balancing the tidal torque from the host star; such a strongly warped disk could be subjected to breaking (Doğan et al. 2015).

In addition to the above considerations, the "observed" gaps in the J1407b disk may halt the propagation of bending waves and cut off viscous torques. Thus, hydrodynamical effects cannot be responsible for the disk's coherence and inclination.

5.3 Implications

The large disk mass [Eq. (31)] required to enforce coherent disk precession or maintain misalignment of the outer disk may be difficult to achieve in the context of circumplanetary disk formation (e.g. Canup & Ward 2006). Moreover, a massive disk can suffer gravitational instability. Evaluating the Toomre Q parameter at the outer radius of the disk, we

Laplace, P. S. 1805, Mecanique C'eleste, Vol. 4 (Paris: Courcier)

Larwood, J. D., Nelson, R. P., Papaloizou, J. C. B., & Terquem, C. 1996, MNRAS, 282, 597

Lehébel, A., & Tiscareno, M. S. 2015, A&A, 576, A92

Lissauer, J. J., & Safronov, V. S. 1991, Icarus, 93, 288

Lubow, S. H., & Ogilvie, G. I. 2000, ApJ, 538, 326

Mamajek, E. E., Quillen, A. C., Pecaut, M. J., et al. 2012, AJ, 143, 72

Martin, R. G., & Lubow, S. H. 2011, MNRAS, 413, 1447

Murray, C. D., & Dermott, S. F. 1999, Solar system dynamics by Murray, C. D., 1999,

Ogilvie, G. I. 1999, MNRAS, 304, 557

Ohta, Y., Taruya, A., & Suto, Y. 2009, ApJ, 690, 1

Papaloizou, J. C. B., & Lin, D. N. C. 1995, ApJ, 438, 841

Papaloizou, J. C. B., & Pringle, J. E. 1983, MNRAS, 202, 1181

Quillen, A. C., & Trilling, D. E. 1998, ApJ, 508, 707

Santos, N. C., Martins, J. H. C., Boué, G., et al. 2015, A&A, 583, A50

Schlichting, H. E., & Chang, P. 2011, ApJ, 734, 117

Tokuda, K., Onishi, T., Saigo, K., et al. 2014, ApJL, 789, L4

Touma, J. R., Tremaine, S., & Kazandjian, M. V. 2009, MNRAS, 394, 1085

Tremaine, S. 1991, Icarus, 89, 85

Tremaine, S., Touma, J., & Namouni, F. 2009, AJ, 137, 3706

Tremaine, S., & Davis, S. W. 2014, MNRAS, 441, 1408

Tusnski, L. R. M., & Valio, A. 2011, ApJ, 743, 97

Ulubay-Siddiki, A., Gerhard, O., & Arnaboldi, M. 2009, MNRAS, 398, 535

Vokrouhlický, D., & Nesvorný, D. 2015, ApJ, 806, 143

van Werkhoven, T. I. M., Kenworthy, M. A., & Mamajek, E. E. 2014, MNRAS, 441, 2845

Ward, W. R. 1981, Icarus, 46, 97

Ward, W. R., & Hamilton, D. P. 2004, AJ, 128, 2501

Zhu, W., Huang, C. X., Zhou, G., & Lin, D. N. C. 2014, ApJ, 796, 67

Zuluaga, J. I., Kipping, D. M., Sucerquia, M., & Alvarado, J. A. 2015, ApJL, 803, L14

APPENDIX: EXACT SELF-GRAVITY TORQUE FOR A CIRCULAR DISK

As noted in Section 3, Eq. (9) is valid only when $|\hat{\boldsymbol{l}}(r') \times \hat{\boldsymbol{l}}(r)| \ll 1$ or $\chi \ll 1$. When $\chi \sim 1$ and $|\hat{\boldsymbol{l}}(r') \times \hat{\boldsymbol{l}}(r)| \sim 1$, a different formalism is needed to compute the torque acting between two circular massive rings. In terms of the warp profile $\hat{\boldsymbol{l}}(r,t)$ and disk surface density $\Sigma(r)$, the specific torque acting on a disk annulus at radius r from the disk's self-gravity is (Kuijken 1991; Arnaboldi & Sparke 1994; Ulubay-Siddiki et al. 2009)

$$\boldsymbol{T}_{\rm sg} = \int_{r_{\rm in}}^{r_{\rm out}} dr' \frac{4\pi G\Sigma(r')}{\max(r,r')} \frac{\chi I(\chi, \sin^2 \alpha)}{(1+\chi^2)^{3/2}}$$
$$\times [\hat{\boldsymbol{l}}(r,t) \cdot \hat{\boldsymbol{l}}(r',t)] [\hat{\boldsymbol{l}}(r,t) \times \hat{\boldsymbol{l}}(r',t)] \quad (44)$$
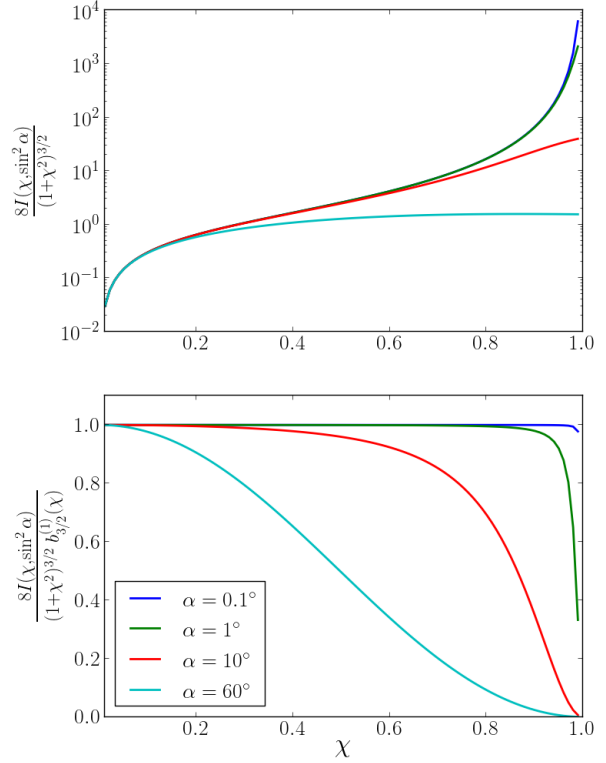

Figure 9. The top panel shows the integrand in Eq. (44) as a function of χ, with values of α as indicated. We remove the dependence on $\sin\alpha\cos\alpha$. The bottom plot shows the ratio of the integrand in (44) and that in (9).

where $\chi = \min(r,r')/\max(r,r')$, $\sin^2 \alpha = |\hat{\boldsymbol{l}}(r,t) \times \hat{\boldsymbol{l}}(r',t)|^2$,

$$I = \frac{4}{\pi^2} \int_0^{\pi/2} d\psi \left[\frac{E(k)(1-k^2/2)}{(1-k^2)} - K(k) \right]$$
$$\times \frac{(1-k^2/2)^{3/2}}{k^2} \frac{\sin^2 \psi}{\sqrt{1-\sin^2 \alpha \sin^2 \psi}} \quad (45)$$
$$k^2 = k^2(\chi, \sin^2 \psi, \sin^2 \alpha)$$
$$= \frac{4\chi\sqrt{1-\sin^2\alpha\sin^2\psi}}{1+\chi^2+2\chi\sqrt{1-\sin^2\alpha\sin^2\psi}} \quad (46)$$

while $K(k)$ and $E(k)$ are elliptic integrals of the first and second kind, respectively. The only approximation used in the derivation of Eq. (44) is that the disk is infinitesimally thin; this formula is exact for arbitrary χ and mutual inclination angles α.

In the top panel of Fig. 9, we plot the integrand in equation (44),

$$\frac{8I(\chi, \sin^2 \alpha)}{(1+\chi^2)^{3/2}}, \quad (47)$$

as a function of χ. We remove the dependence of $\sin\alpha\cos\alpha$, as they are already present in our approximation (9). We see that when $|\alpha| > 0$, the integrand (47) becomes large but stays finite as $\chi \to 1$. In the bottom panel of Fig. 9, we plot

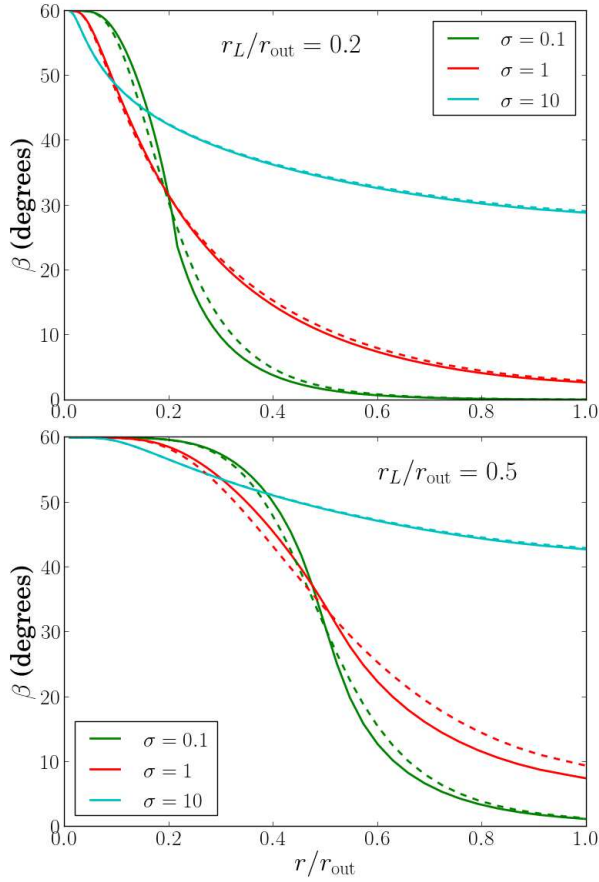**Figure 10.** Equilibrium disk inclination profile $\beta(r)$ including the effect of self-gravity for different values of $r_L/r_{\rm out}$ and σ [see Eq. (20)] as indicated. The results obtained using the approximate self-gravity torque [Eq. (9)] are shown in dashed lines, while those obtained with the exact self-gravity torque [Eq. (44)] are shown by solid lines. We take $p = 1.5$ [Eq. (12)] and $\beta_{\rm p} = 60°$ for all solutions.

the ratio of the integrands in Eqs. (44) and (9),

$$\frac{8I(\chi, \sin^2\alpha)}{(1+\chi^2)^{3/2}\, b_{3/2}^{(1)}(\chi)}. \tag{48}$$

Since the quantity (48) is approximately unity for most of the parameter range of interest (Fig. 9), we do not expect significant corrections to the equilibrium disk warp profiles obtained in Section 3.

We have repeated the calculation of the Laplace equilibria for disk warp profiles using the exact torque expression (44). Figure 10 shows a sample of our numerical results for the disk inclination profile $\beta(r)$, with $\Sigma \propto r^{-3/2}$ and the values of σ and $r_L/r_{\rm out}$ as indicated. The solutions for $\beta(r)$ with the approximate torque expression (9) are also shown for comparison. We see that using the exact self-gravity torque (44) changes the solution of the equilibrium disk warp $\beta(r)$ by less than a few degrees in all cases.